Congchun Chen [1], Yu-qin Long [2], Zhihong Shi [3], Jiarong Zhao [4]

УДК 624.012.4:519.6

[1–4] School of Urban Construction and Safety Engineering, Shanghai Institute of Technology, Shanghai, China

FINITE ELEMENT ANALYSIS OF THE AXIAL COMPRESSION PERFORMANCE OF 3D-PRINTED ULTRA-HIGH PERFORMANCE CONCRETE AND CAST-IN-PLACE CONCRETE COMPOSITE SHORT COLUMNS

Concrete 3D printing construction technology is a new green construction technology with broad application prospects. At this stage, more research on the mechanical properties of concrete 3D-printed structures still needs to be done. This paper investigates the effect of printing layer thickness on the axial compressive mechanical properties of composite short columns through finite element analysis of the stress-strain of 3D printed ultra-high performance concrete and cast-in-place concrete composite short columns under axial load. The results show that the printed shell can effectively restrain the internal core concrete; under axial compression, the reduction in the thickness of the printed layer leads to a decrease in the ductility of the short column while the compressive strength is improved. It provides a reference for practical engineering and subsequent research.

Keywords: 3D printing; ultra-high performance concrete; concrete composite short column; finite element analysis.

For citation: Congchun Chen & Yu-qin Long & Zhihong Shi & Jiarong Zhao. Finite Element Analysis of the Axial Compression Performance of 3D-printed Ultra-high Performance Concrete and Cast-in-Place Concrete Composite Short Columns. Sophia. 2025;1:40–53. English.

Конгчунь Чэнь [1], Юй-цинь Лун [2], Чжихун Ши [3], Цзяжун Чжао [4]

[1–4] Факультет городского строительства и техники безопасности, Шанхайский технологический институт, Шанхай, Китай

КОНЕЧНО-ЭЛЕМЕНТНЫЙ АНАЛИЗ ХАРАКТЕРИСТИК ОСЕВОГО СЖАТИЯ КОРОТКИХ КОЛОНН ИЗ КОМПОЗИТНОГО СВЕРХВЫСОКОПРОЧНОГО БЕТОНА И МОНОЛИТНОГО БЕТОНА, ИЗГОТОВЛЕННЫХ МЕТОДОМ 3D-ПЕЧАТИ

Технология строительства с использованием 3D-печати бетоном представляет собой новую экологичную строительную технологию, имеющую широкие перспективы применения. На данном этапе все еще необходимо провести больше исследований механических свойств конструкций, созданных с помощью 3D-печати бетоном. В данной статье исследуется влияние толщины печатного слоя на осевые сжимающие механические свойства композитных коротких колонн путем анализа методом конечных элементов напряженно-деформированного состояния ультра-высокопрочного бетона, напечатанного на 3D-принтере, и монолитных бетонных композитных коротких колонн под осевой нагрузкой. Результаты показывают, что напечатанная оболочка может эффективно сдерживать внутренний сердечник из бетона; при осевом сжатии уменьшение толщины печатного слоя приводит к снижению пластичности короткой колонны, в то время как прочность на сжатие повышается.

Это предоставляет ориентиры для практического применения в инженерных проектах и последующих исследований.

Ключевые слова: 3D-печать; ультра-высокопрочный бетон; бетонная композитная короткая колонна; анализ методом конечных элементов.

Образец цитирования: Конгчунь Чэнь. Конечно-элементный анализ характеристик осевого сжатия коротких колонн из композитного сверхвысокопрочного бетона и монолитного бетона, изготовленных методом 3D-печати / Конгчунь Чэнь, Юй-цинь Лун, Чжихун Ши, Цзяжун Чжао // София: электрон. науч.-просветит. журн. – 2025. – № 1. – С. 40–53.

Авторы:

[1] **Чэнь Конгчунь** – старший инженер, доцент Уханьского технологического университета; докторская степень в Университете Тунцзи по специальности «Мостовое и туннельное строительство». Работает в Шанхайском технологическом институте.

chencongchun@163.com

Authors:

Chen Congchun – senior engineer, associate professor Wuhan University of Technology; a doctorate Tongji University in 2006 with in Bridge and Tunnel Engineering. Working at Shanghai Institute of Technology.

[2] **Юй-цинь Лун** – магистрант Школы городского строительства и инженерной безопасности Шанхайского технологического института. Ее исследования сосредоточены на укреплении бетонных конструкций.

2456967444@qq.com

Yu-qin Long – currently a Master's student at the School of Urban Construction and Safety Engineering, Shanghai Institute of Technology. Her research focuses on the strengthening of concrete structures.

1. Introduction

Concrete 3D printing construction technology, as a highly automated and flexible construction technology emerging in recent years, is based on three-dimensional digital models and completes the construction of the target structure by printing and stacking layers of material on top of each other [1; 2]. Each building or component can be personalized on demand using the contouring process in the 3D printing technology [3] approach. Ultra High-Performance Concrete (UHPC) has excellent physical and mechanical properties and is widely used in engineering and construction [4]. In this paper, the two are combined to study the force performance of 3D printed ultra-high performance concrete and cast-in-place concrete composite short columns, using finite element software to simulate them and adjusting the

thickness of the printing layer from the printing process to analyze the effect of the two on the axial compression performance of the composite structure, and to provide theoretical support for the application of practical engineering.

2. Finite element eigenmodel

General-purpose finite element software was selected, and the principal structures, cell types, and contact conditions used were further refined by 3D printing of specimen simulations of each anisotropy with parameter inputs for the interlayer cohesive cell.

2.1. Plastic damage modelling of concrete

The plastic damage model for concrete in this finite element software assumes that the material has isotropic damage, applies to concrete under various loads, including cyclic and dynamic loads, and takes into account the degradation of elastic stiffness due to tensile and compressive plastic strains as well as the stiffness recovery in the unloaded state [5]. The results of this study are summarised in the following table.The stress-strain relationships for the damage plasticity model of concrete in compression and tension in the finite element software are shown in *Fig 1* and *Fig 2*.

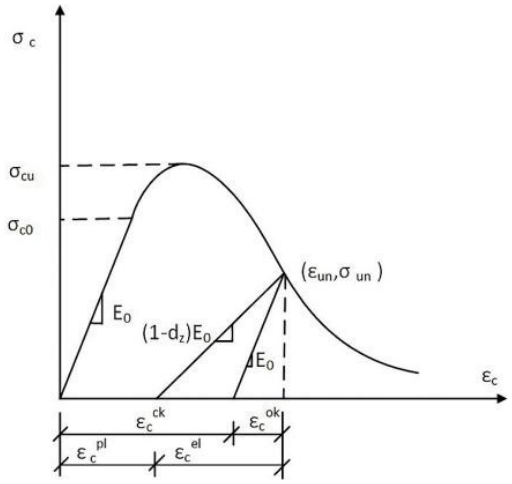

Fig. 1. Compressive stress-strain curve of concrete damage plastic model.

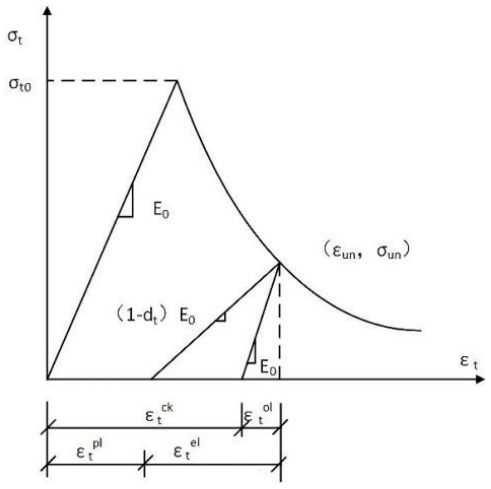

Fig. 2. Tensile stress-strain curve of concrete damage-plastic model.

2.2. Selection of normal C30 concrete material eigenstructure

The selection of C30 concrete principal structure follows China's "Code for the Design of Concrete Structures" (GB50010-2010) [6]. The uniaxial stress-strain curve is shown in *Fig. 3*.

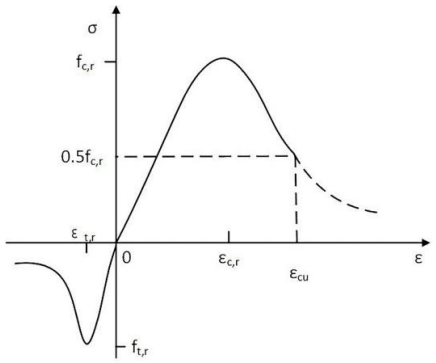

Fig. 3. Uniaxial stress-strain curve of concrete.

2.3. Selection of reinforcing steel principal structure

The stress-strain constitutive relationship of single loading of steel reinforcement adopts the ideal completely elastic-plastic bilinear model, as shown in *Fig. 4*.

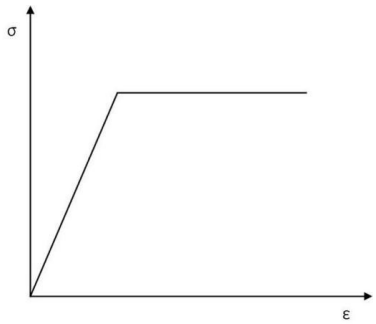

Fig. 4. Stress-strain curves of steel bars.

2.4. Selection of reinforcing steel principal structure

Uniaxial compression and tension of UHPC [7–10] and tension [11]. The stress-strain ontological relationship is selected as shown in *Fig. 5* and *Fig. 6*.

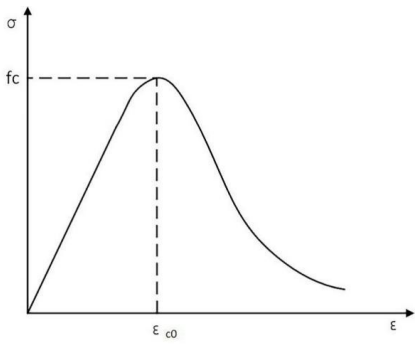

Fig. 5. UHPC uniaxial compressive stress-strain curve.

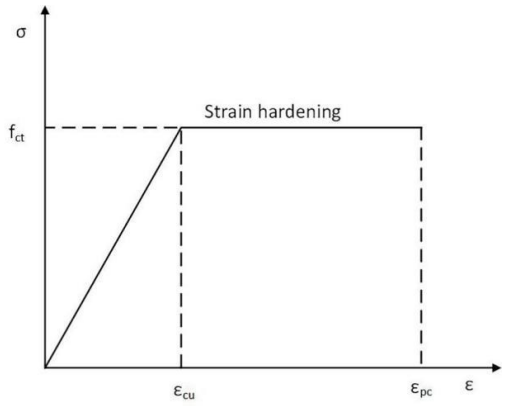

Fig. 6. UHPC uniaxial tensile stress-strain curve.

In the finite element software, CDP model materials also need to enter several parameters; in this paper, to facilitate the subsequent simulation, it is easy to converge references [12; 13]. The selected parameters are shown in *Table 1* below.

Table 1

CDP model material parameter table

Expansion angle	***Eccentricity***	***fb0/fc0***	***K***	***Viscosity parameter***
36°	0.1	1.16	0.6667	0.0005

3. Simulation overview

3.1. Loading method

The calculation is complex to converge because the concrete material is nonlinear in finite element analysis. In this paper, displacement-controlled loading is used in the simulation to ensure that the model can converge better; at the same time, in order to facilitate the control, the reference point RP-1 is established first, and the point is coupled with the upper surface of the short column, which is completely fixed to the lower surface of the core concrete and UHPC layer. The test adopts a monotonic loading system; the loading rate is 0.5 mm/min, and it is agreed that the test ends when the load is reduced to 60 % of the maximum load.

3.2. Specimen design

This simulation will be for a group of three printed single-layer thickness of 20 mm, 40 mm, 50 mm width of 50 mm ultra-high performance concrete 3D printed short columns, a group of three printed single-layer width of 30 mm, 40 mm, 50 mm thickness of 50 mm ultra-high performance concrete 3D printed short columns, and a short column of the exact dimensions of the ordinary cast C30 reinforced concrete as shown in *Fig. 7*. The dimensions of all the short concrete columns are 250 mm radius and 1000 mm height, and the ultra-high performance concrete 3D printed short columns are printed using the contour process; firstly, the external shell is printed with the specifications of the outer diameter D = 600mm and the inner diameter d = 500 mm, and then the shell is printed with the rebar cage embedded in the shell to be formed by pouring the C30 concrete. Reinforcement cage hoop selection of 6mm diameter HPB300 rebar, hoop spacing of 150 mm for a total of 6, the longitudinal bar for the diameter of 12 mm HPB300 rebar for a total of four.

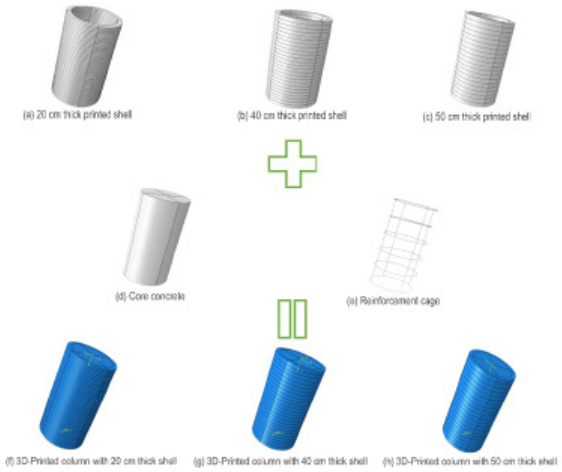

Fig. 7. Schematic diagram of 3D printing short column structure.

The material parameters of the above structure are shown in *Table* 2.

Table 2

Material parameter table

Component	***Material***	***Modulus of elasticity (MPa)***	***Tensile strength (MPa)***	***Prism compressive strength (MPa)***	***Poisson's ratio***
Reinforcement layer	1.5% UHPC	50100	5.6	115.1	0.2
Hoop reinforcement	HPB300/d8	2.06×105	256	/	0.3
Longitudinal reinforcement	HRB300/d12	2.06×105	270	/	0.3
Ordinary concrete	C30	30000	2.82	28.82	0.2

3.3. Cell division

In this paper, the C3D8R (three-dimensional eight-node reduced integral) unit is used for the reinforcement layer and C30 concrete, the C0H3D8 (three-dimensional eight-node solid) unit is used for the cohesive bonding layer between the printed shell layer and the layer, and T3D2 (two-node linear truss) unit is used for the reinforcing steel.The cohesive bonding unit is used to connect the contact printing layer with the layer, and after setting a reasonable bond strength, the two are subjected to the force together. The reinforcement layer and the core concrete are connected by “face-to-face contact”, and the “penalized contact”-function with a friction coefficient of 0.5 is selected for tangential behavior, while the “hard contact” function is selected for normal pressure behavior. The “hard contact” function is selected for the tangential behavior. Reinforcing bars are embedded in the center of the cast concrete using the built-in embedded command.The schematic diagram of the cell division of the component is shown in *Fig. 8*.

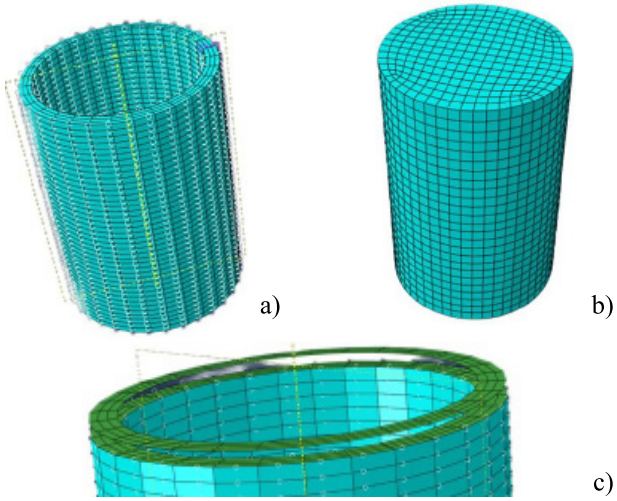

Fig. 8. Schematic diagram of component cell division: a) Printed shell mesh model; b) Core cast concrete mesh model; c) Schematic diagram of cohesive cells in the intermediate bond layer.

4. Analysis of simulation results

4.1. Analysis of specimen stress-strain maps

4.1.1. Cloud diagram of reinforcement cage

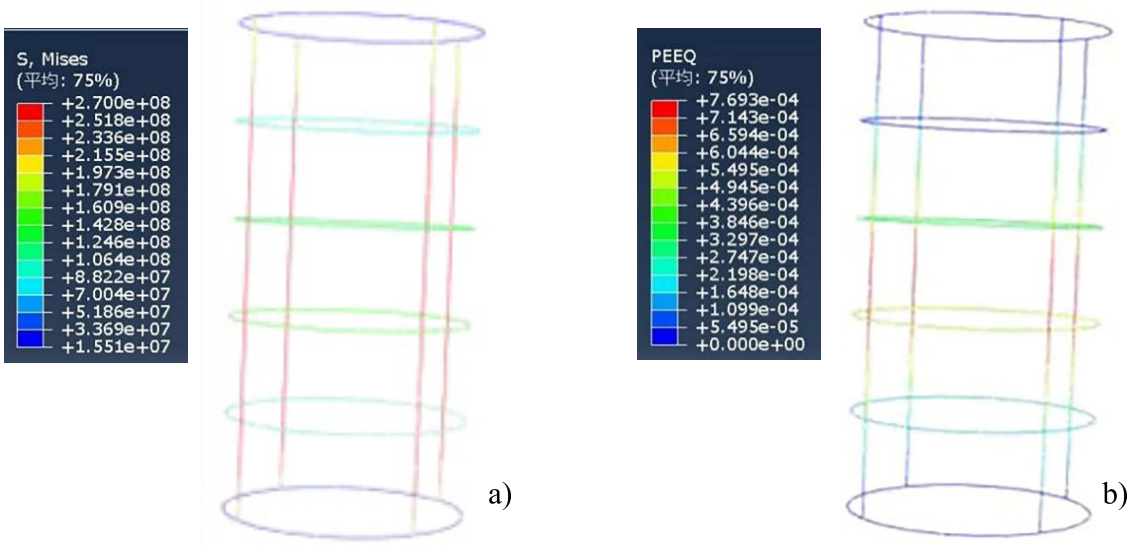

Fig. 9. Axial rebar cage cloud diagram: a) Stress diagram of reinforcement cage at the time of damage; b) Strain diagram of rebar cage during damage

As shown in *Fig. 9* of the cage cloud diagram, the stress strain of the longitudinal bars of the cage is much larger than that of the hoop bars after the load is applied. The stress-strain in the middle of the longitudinal bars is the largest. The damage also occurs in the middle of the longitudinal bars of the steel fibers so that the stress and damage of the cage of a short concrete 3D printed column are similar to that of an ordinary poured concrete short column.

4.1.2. Printed shell cloud diagram

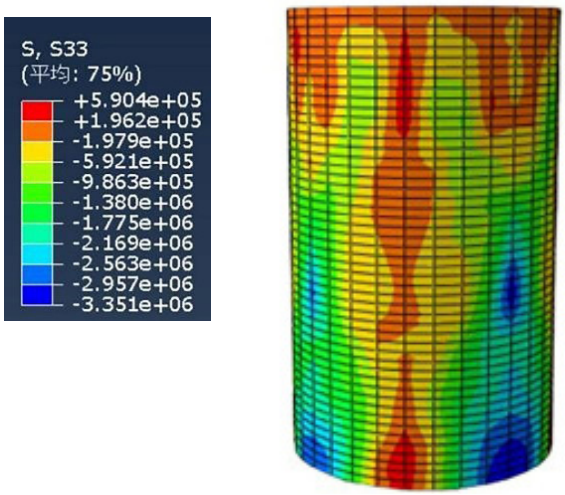

a)

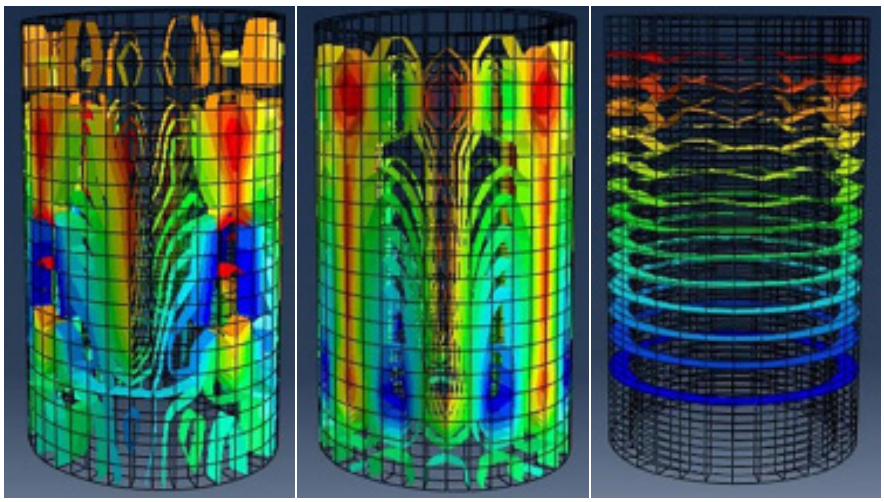

b)

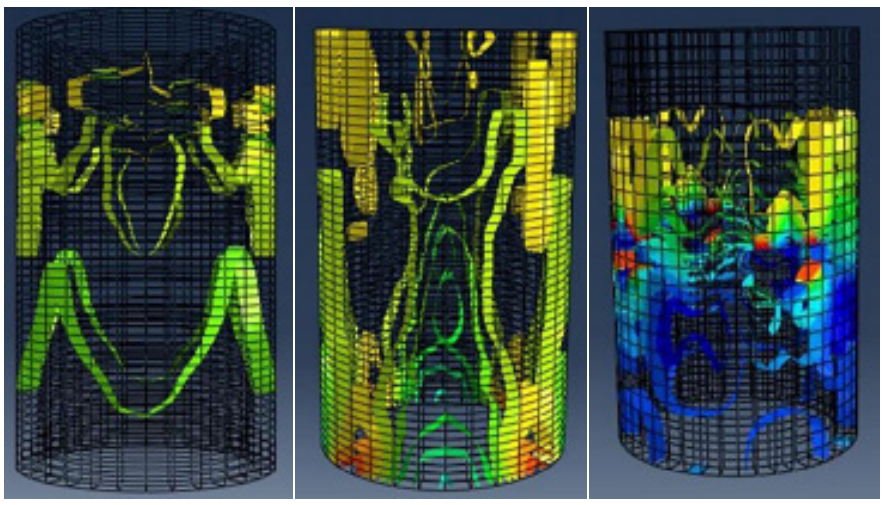

c)

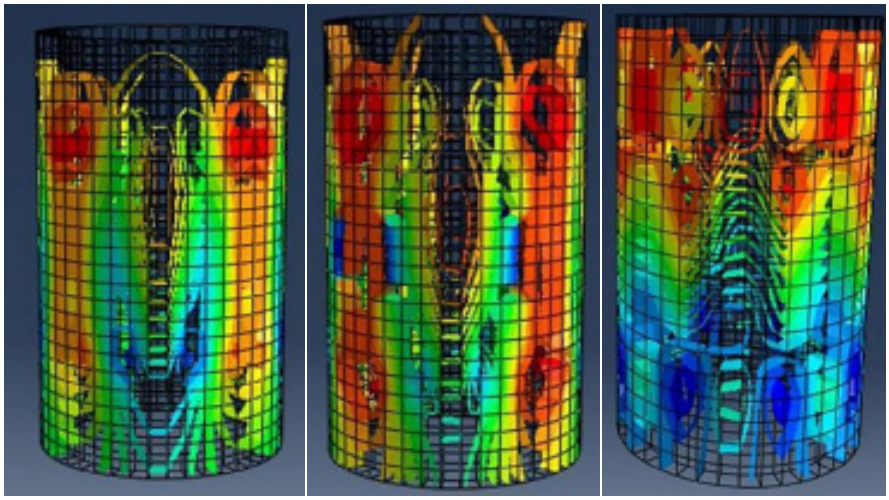

d)

Fig. 10. Print the axial stress contour of the shell: a) Schematic of the stress cloud of printed shells;
b) C3DP-20 printed shell stress cloud equivalent surface map;
c) C3DP-40 print shell stress cloud diagram equivalent surface map;
d) C3DP-50 Print the axial stress map equivalent surface map.

As shown in *Fig. 10* of the printed shell, after loading the 3D printed shell, the stress first rises on the top and bottom surfaces and then passes to the middle. When the stress cloud mode is selected to display the contour surface, it is found that the stress contour surface of the printed layer from 20 mm to 50 mm is continuously encrypted, and the stress contour surface of 20 mm develops rapidly in the longitudinal direction. It is assumed that the cracks may expand faster in the 20 mm single-layer printing thickness, but more cracks appear in the 40 mm and 50 mm single-layer printing thicknesses. The reason for this may be that the 20 mm print layer shell has more bonded surfaces, and the steel fibers inside the UHPC material used for printing do not play a good role in bridging the cracks, and the steel fibers are more likely to line up in the direction of printing.

4.1.3. Core concrete cloud diagram

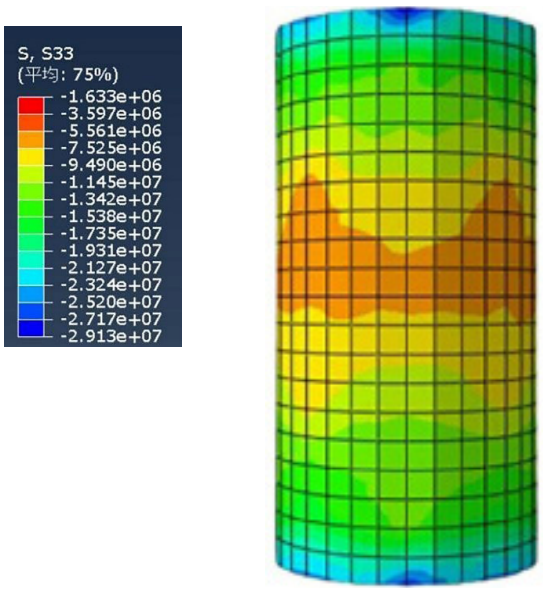

a)

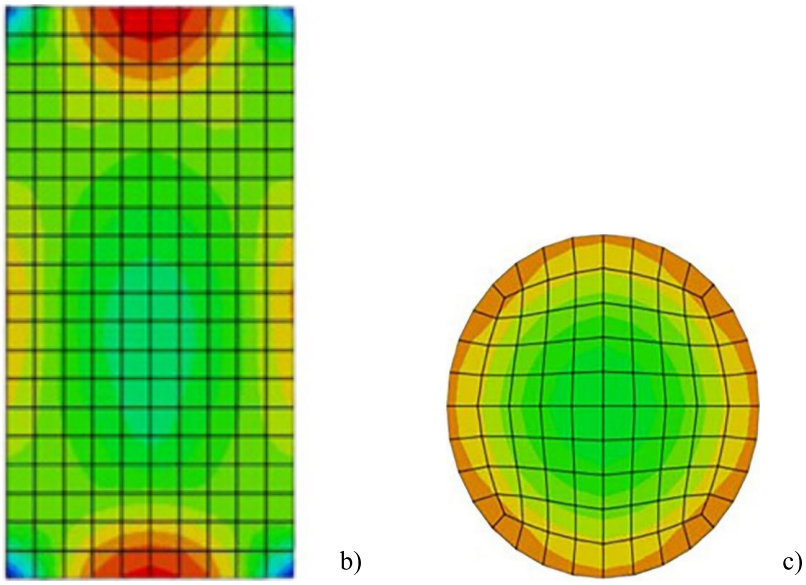

Fig. 11. Core concrete stress contour: a) Stress cloud of core concrete; b) Vertical section stress contour; c) Horizontal section stress contour.

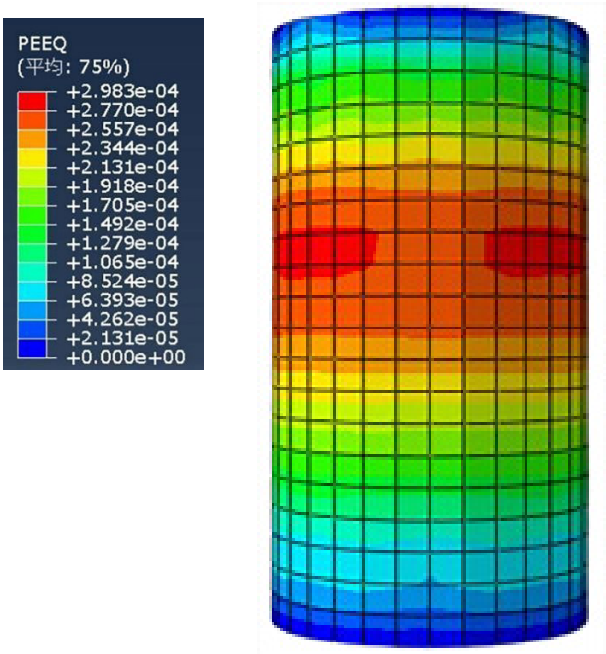

Fig. 12. Strain cloud map of core concrete.

As illustrated in *Fig. 11* and *Fig. 12*, it is evident that under loading conditions, the stress at the ends of the core concrete cylinder is relatively lower compared to the higher stress concentration observed in the central region of the column. The stress distribution exhibits symmetry about the central axis, and the binding force of the outer printed shell intensifies following significant strain in the midsection of the core concrete column. On the transverse plane, the stress within the core concrete is approximately distributed in a ring pattern, with a gradual decrease from the periphery towards the center.

4.1.4. Cloud diagram of 3D printed composite short column with ultra-high performance concrete

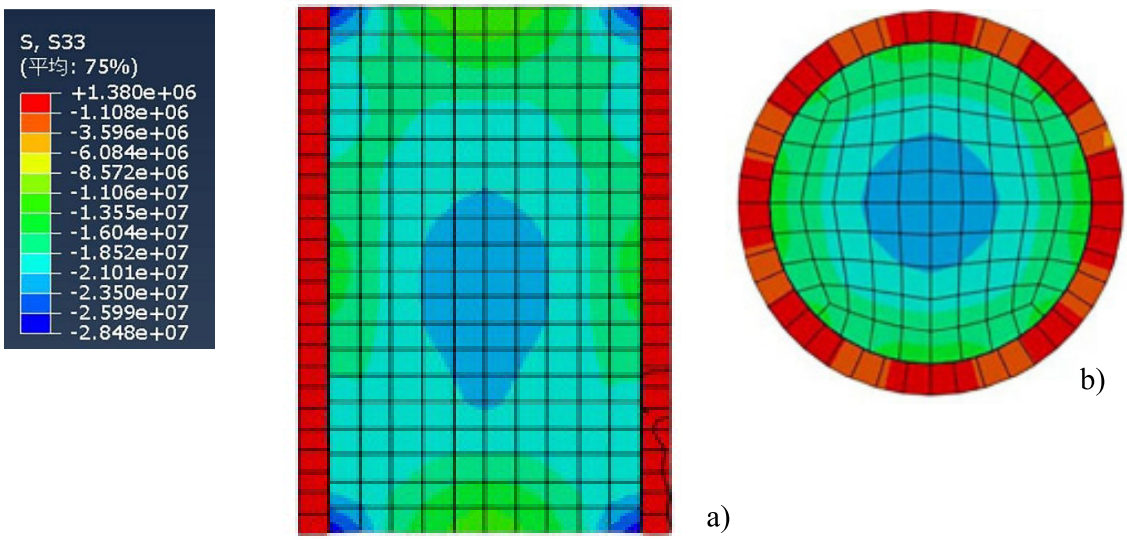

Fig. 13. Stress Distribution in Ultra-High Performance Concrete 3D Printed Short Columns: a) Vertical section stress contour; b) Horizontal section stress contour.

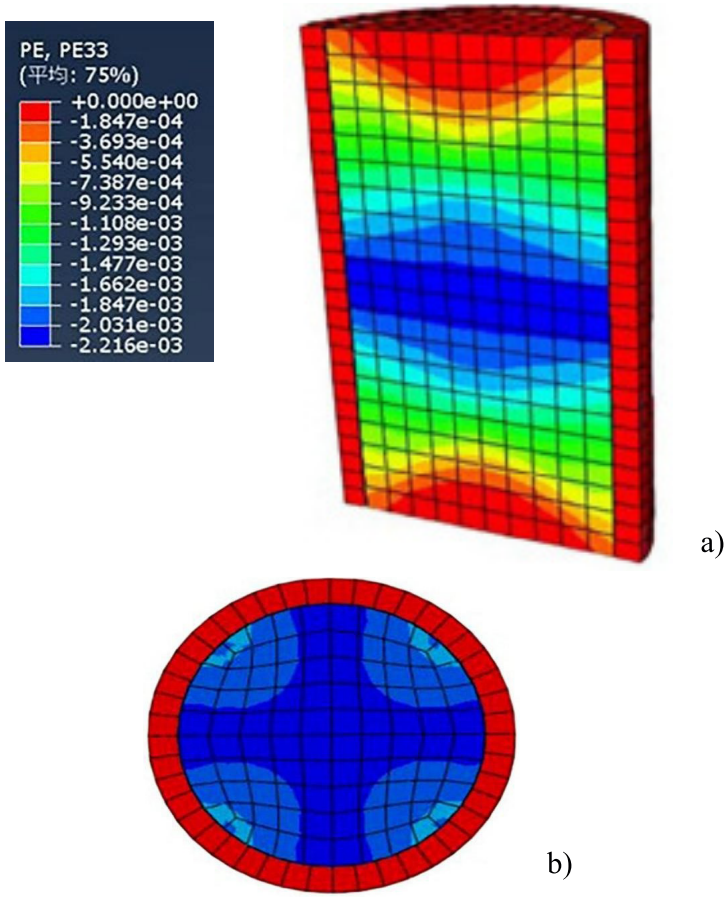

Fig. 14. Strain Cloud Image of a 3D-Printed Ultra-High Performance Concrete Short Column: a) Vertical section strain maps; b) Horizontal section strain contour.

As shown in *Fig. 13* and *Fig. 14* of the stress cloud of the composite short column, the stress strain of the external shell of the printed column is much larger than that of the internal core concrete after axial loading, which indicates that the printed shell has a better restraining force on the internal core concrete. The damage to the member will also start from the damage of the external shell until spalling failure.

4.2. Peak load and displacement

Finite element analysis is carried out for the above ultra-high performance concrete 3D printed short column and ordinary C30 cast reinforced concrete short column models; the load-displacement curves are shown in *Fig. 15*, and the calculated peak load-limit displacements are shown in *Table 3*. Combined with the graphs, the analysis concludes that the strength of all three types of ultra-high performance concrete 3D printed short columns is lower than that of cast-in-place concrete short columns. Among them, the peak load of 20 mm ultra-high performance concrete 3D printed short columns is the highest, the peak load of 40 mm ultra-high performance concrete 3D printed short columns is the second highest, and 50 mm ultra-high performance concrete 3D printed short columns is the lowest, and the peak loads of the three ultra-high performance concrete 3D printed short columns are decreased by 12.4 %, 23.4 %, and 28.6 % compared with that of cast-in-place concrete short columns, respectively. Overall, the peak load of the ultra-high performance concrete 3D printed short columns decreases gradually with the increase of the thickness of the printed layer.

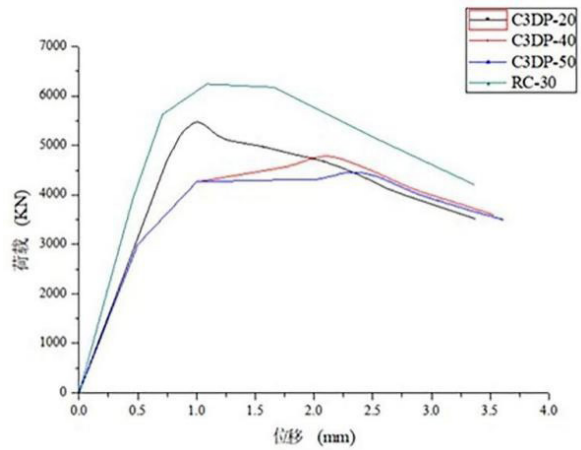

Fig. 15. Load-displacement curve of each short column.

Table 3

Component Peak Load-Displacement Table

member	*peak load (KN)*	*peak displacement (mm)*	*limit displacement (mm)*
C3PD-20	5468.76	1.01	1.329
C3PD-40	4781.67	2.12	2.916
C3PD-50	4459.18	2.27	3.188
RC-30	6244.56	1.09	2.268

4.3. Ductility effects

To evaluate the ductility of short columns 3D printed with ultra-high performance concrete, the ductility index (DI) method is adopted [14]. DI is equal to the displacement ratio corresponding to the peak load and declines to 85 % of the peak load [15; 16], which can describe the ductility of the structural section, as shown in *Formula 1*.

$$DI = \frac{\Delta_{85\%}}{\Delta_u} \quad 1)$$

From the above formula, the ductility indices of C3PD-20, C3PD-40, C3PD-50, and RC-30 are 1.32, 1.38, 1.40, and 2.08, respectively, which shows that the ductility indices (DI) of the three types of ultra-high-performance concrete 3D-printed short columns are lower than those of the poured ordinary concrete short columns. The thickness of the printing layer is 40 mm and 50 mm from the load-displacement curves. The ultra-high-performance 3D printed short columns have greater damage displacement and deformation than the poured ordinary concrete short columns. However, the ultra-high-performance concrete 3D-printed short columns will be destroyed quickly after the print shell is damaged and spalled. Meanwhile, the ductility of the UHP concrete 3D printed columns decreases with the thickness of the printed layer. The reason may be the damage to the printed shell at the weak point of the interlayer bond, which leads to the spalling of the printed shell.

According to the curve, the failure of the short column of ultra-high performance concrete 3D printing under load is inferred. The printing shell of the short column of ultra-high performance concrete 3D printing on the 20 mm printing layer and the reinforced concrete poured inside are under good joint stress. Moreover, due to the small thickness of the printing layer and the good orientation and distribution of steel fibers, the printing matrix has strong toughness. However, at the same time, the smaller thickness of the printing layer requires more layers when printing the shell, which will result in more interlayer bonding. Once a layer of the printing body is cracked and destroyed, the entire shell will be quickly damaged. For 40 mm and 50 mm thick ultra-high performance concrete 3D printed short columns, when cracks appear in the printed body, they can continue to work with cracks for some time. With the destruction and spalling of the printed shell, the final ultra-high performance concrete 3D printed short column is loaded with the poured reinforced concrete in the center, so in the final stage, RC-30 has the same curve downward trend.

5. Summary

1) The print shell has a good binding force on the internal core concrete.
2) The ductility of short 3D printed columns of ultra-high performance concrete in axial compression decreases with the reduced thickness of the printed layer. At the same time, the structure's compressive strength increases with the reduced thickness of the printed layer.
3) At present, the axial compressive strength of 3D-printed components is not as good as that of integrated casting components; this conclusion needs to be tested by experiment.

REFERENCES

1. *Chao*, *Z.*, *Zhicong*, *D.*, *Zeyu*, *H.*, *Chun*, *C.*, *Yamei*, *Z.*: Research progress of concrete 3d printing. Industrial Building 50(08), 16–21 (2020) https://doi.org/10.13204/j. gyjzG20052510.

2. *Baoshan*, *L.*, *Yiming, Y.*, *Cong*, *L.*: Research progress on mechanical properties of extruded 3d printed concrete. Concrete and Cement Products (03), 1–6 (2021) https://doi.org/10.19761/j.1000-4637.2021.03.001.06.

3. *Ma G W*, *J. Y. Wang L*: State-of-the-art of 3d printing technology of cementitious material—an emerging technique for construction. Science China Technological Sciences 61(04), 475–495 (2018) https://doi.org/10. 1007/s11431-016-9077-7.

4. *Xinlei*, *C.*, *Rui*, *M.*, *Xiaoying*, *L.*: Research progress on preparation and mechanical properties of ultra-high performance concrete. Silicate Bulletin 43(12), 4295–4312 (2024) https://doi.org/10.16552/j.cnki.issn1001-1625.20240816.001.

5. *Lianbo*, *T.*, *Jianguo*, *H.*: Research on reasonable value of plastic damage factor of concrete in abaqus. Journal of Hubei University (Natural Science Edition) 37(04), 340–345358 (2024).

6. Code for the design of concrete structures. Construction Industry Press (2010).

7. *Pinwu*, *G.*, *Yazheng*, *T.*, *Pu*, *Z.*, *Guobin*, *T.*: Research on uniaxial tension-compression principal relationship of ultra-high performance concrete. Journal of Composite Materials 36(05), 1295–1305 (2019) https://doi. org/10.13801/j.cnki.fhclxb.20180703.004.

8. *Bo*, *S.*: Test and research on the basic mechanical properties of activated powder concrete. Master's thesis, Hunan University (2002).

9. *Youming*, *W.*: Study on stress-strain full curve of reactive powder concrete (rpc) under compression. Master's thesis, Hunan University (2007).

10. *T*, *S.*: Research on uniaxial compression principal relationship and structural design parameters of activated powder concrete. Master's thesis, Harbin Institute of Technology (2014).

11. *Zhe*, *Z.*: Research on bending and tensile performance of steel-reinforced uhpc combined bridge deck structure. Master's thesis, Hunan University (2016).

12. *Hao-yu*, *L.*: Identification of parameters and finite element validation of plastic damage constitutive model for rpc materials. Master's thesis, Beijing Jiaotong University (2009).

13. *Zongcai*, *D.*, *Yichao*, *W.*, *Rui*, *X.*: Experimental study and theoretical analysis of flexural performance of uhpc beams with high strength steel reinforcement. Journal of Applied Basic and Engineering Sciences 23(01), 68–78 (2015) https://doi.org/10.16058/j.issn.1005-0930.2015.01.006.

14. *Yan*, *J.-B.*, *Wang*, *X.-T.*, *Wang*, *T.*: Compressive behaviour of normal weight concrete confined by the steel face plates in scs sandwich wall. Construction and Building Materials 171, 437–454 (2018) https://doi.org/10.1016/j.conbuildmat.2018.03.143.

15. *Li*, *P.*, *Zhang*, *T.*, *Wang, C.*: Behavior of concrete-filled steel tube columns subjected to axial compression. Advances in Materials Science and Engineering 2018(1), 4059675 https://doi.org/10.1155/2018/4059675.

16. *Ge*, *H.*, *Usami*, *T.*: Cyclic tests of concretefilled steel box columns. Journal of Structural Engineering 122(10), 1169–1177 (1996) https://doi.org/10.1061/(ASCE)0733-9445(1996)122:10(1169).